Korean J. Chem. Eng., 37(6), 946-954 (2020)
DOI: 10.1007/s11814-020-0533-2

pISSN: 0256-1115
eISSN: 1975-7220

A novel ternary Pd-GO/N-doped TiO_2 hierarchical visible-light sensitive photocatalyst for nanocomposite membrane

Hossein Mahdavi†, Mahdi Rezaei, Leila Ahmadian-Alam, and Mostafa Mohammadpour Amini

School of Chemistry, College of Science, University of Tehran, P.O. Box 14155-6455, Tehran, Iran
(*Received 8 December 2019 • accepted 5 March 2020*)

Abstract−We investigated the visible-light sensitive photocatalytic ability of a designed ternary Pd-GO/TiON nanocomposite for use as an effective photocatalyst in membranes. We succeeded in synthesizing the TiO_2-based photocatalyst for Suzuki coupling reaction and application of this photocatalyst for fabricating high performance photocatalytic membrane. In this regard, palladium metal as a complementary metal in combination with N-doped TiO_2 (TiON) and graphene oxide (GO) nanosheets was utilized to synthesize the upgraded version of the visible light sensitive nanocomposite photocatalyst. The synthesis of Pd-GO/TiON hierarchical nanostructure was confirmed by detecting Ti, Pd, C, O and N elements by X-ray photoelectron spectroscopy (XPS), energy dispersive X-ray (EDX) and EDX mapping analysis. Then, a series of PVDF-based photocatalytic nanocomposite membranes (PhNMs) filled with Pd-GO/TiON was fabricated. Evaluating the yield of Pd-GO/TiON photocatalyst was around 99% and 70% for heterogeneous system and the prepared PhNM containing 3% Pd-GO/TiON, respectively. Although, yield of Pd-GO/TiON photocatalyst in membrane is not comparable with the high yield reported by other researchers in heterogeneous system; however, it can be considered as a valuable result because of the importance of photocatalytic reactions and the environmental advantages of membrane technology. Furthermore, various analyses were also performed to study the synthesized photocatalysts and the prepared photocatalytic membranes, including thermogravimetric analysis (TGA), scanning electron microscopy (SEM), X-ray powder diffraction (XRD) and diffuse reflectance spectrophotometry (DRS).

Keywords: Photocatalytic Membrane, Palladium, N-doped TiO_2, Graphene Oxide, Polyvinylidene Fluoride

INTRODUCTION

In the past, membranes were usually made by ceramic and metallic materials. However, nowadays polymeric membranes, which are less concentrated than inorganic ones, have drawn considerable attention for their low cost and high proficiency [1]. Polymeric nanocomposite membranes are contrasted with the traditional polymeric membranes in view of their enhanced properties [1]. Most famous polymeric nanocomposite membranes were prepared by graphene or graphene with functional groups (e.g., graphene oxide) [2], metal oxides [3], zeolites [4], carbon nanotubes [5,6] and C60 [7]. Catalytic reactions, among the most important reactions in industrial processes such as chemical industry, energy conversion and waste water treatment, have also been considered in PNMs [8].

A membrane as a multiple-phase reaction framework which can effectively separate reaction materials like products and catalysts is one of the interesting research subjects in chemical synthesis [9]. Recovery and reuse of catalyst are the fundamental issues in catalytic reactions [10,11]. Therefore, the utilization of catalytic membrane reactors (CMRs) as an important part of membrane technology has been considered to compensate the aforesaid problems [11,12]. By introducing CMRs, metallic catalysts, especially intermediate metals embedded into polymeric membranes, can be effectively used several times [9]. Thus, nowadays, polymeric catalytic membrane is known as a momentous efficiency path for C-C cross-coupling in multiple-phase strategies. Development and improvement of multiple-phase reaction frameworks such as CMRs for Suzuki reactions would provide an extensive variety of utility in synthetic chemistry, whereas organic synthesis is ordinarily performed by mixing solutions [13]. To our knowledge, there is no comprehensive investigation of using photocatalyst in the CMRs; however, membrane technology combined with photocatalyst has been used for purification of wastewater [14].

TiO_2 has been widely used as a photocatalyst due to good chemical stability, acceptable photoactivity and economic efficiency, more than all semiconductors [15]. However, TiO_2 needs to be modified because the photocatalytic properties of TiO_2 can only be seen at wavelengths less than 400 nm [15,16]. According to the literature reviewed, anion doping of TiO_2 with B-, P-, S-, F-, and N-elements has been reported as promising for improving visible-light sensitive photocatalytic ability of TiO_2 [17,18]. However, anion doping resulted in the massive charge carrier recombination, which dramatically declined the photocatalytic activity of anion-doped TiO_2 under visible light illumination. Therefore, using carbon compounds category, including multi-walled carbon nanotubes, GO and graphene, has been introduced to improve the photocatalytic activity of anion-doped TiO_2 [19]. Thus, in introducing this work, taking advantage of the unique electronic properties of the GO, we expect that the combination of GO with visible-light sensitive photocatalyst (N-doped TiO_2) may induce interesting charge transfer and thus

†To whom correspondence should be addressed.
E-mail: hmahdavi@khayam.ut.ac.ir
Copyright by The Korean Institute of Chemical Engineers.

enhance the photocatalytic activity of that. The Suzuki coupling reaction can be mentioned as one of the most important representatives of the palladium-catalyzed reactions. In recent years, several reports have been published on the effects of palladium (Pd) derivatives, such as palladium oxide on the photocatalytic properties of TiON [20,21]. Although, metals such as nickel plus palladium have been used as photocatalyst for the Suzuki coupling reaction [19], there is no specific report on the study of the Suzuki reaction using photocatalytic properties of TiON. According to important functional traits of palladium for Suzuki reactions, it is anticipated that utilizing palladium element in combination with N-doped TiO_2 and GO can be an effective way to enhance the proficiency of TiO_2 photocatalyst for Suzuki reaction, because this noble metal can optimize the transfer pathway of photogenerated electrons across the interface of GO and N-doped TiO_2 photocatalyst. Furthermore, noble metals can also be utilized as electron reservoir to delay the recombination of photogenerated electron-hole pairs of photocatalysts [19].

PVDF is an interesting polymer for use as a membrane because of its great film forming, high chemical resistance to acids, oxidative stability, thermal stability, and good mechanical properties [22]. Therefore, we fabricated photocatalytic nanocomposite membranes by PVDF and photocatalyst agents including Pd/TiON and Pd-GO/TiON for the Suzuki reaction. To attain the photocatalytic ability of TiO_2 in the visible region, nitrogen doping of TiO_2 was performed [18]. In addition, to improve the electron transfer efficiency and lifetime of photogenerated electrons of photocatalyst, graphene oxide nanosheets, which include good properties such as good surface electrons, high electron conductivity, large surface area, and high adsorption capacity, were used to synthesize a TiO_2-based photocatalyst [23]. It is expected that the positive effects of the GO nanosheets along with palladium improve the photocatalytic activity, thereby raising the yield of the Suzuki reaction.

EXPERIMENTAL

1. Materials

PVDF (Hylar_ 5000) was purchased from Elf Atochem, UK. Graphite flakes (Aldrich), sulfuric acid (H_2SO_4, Merck, 98%), nitric acid (HNO_3, Merck, 99%), potassium permanganate ($KMnO_4$, Merck, 99%), sodium dodecyl sulfate (SDS, Aldrich, 98%), iodobenzene (Aldrich, 98%), 4-iodoanisole (Aldrich, 98%), 1-naphthalenebronic acid (Aldrich, 95%), phenylboronic acid (Aldrich, 95%), potassium carbonate (Aldrich, 99.99%), titanium tetrachloride ($TiCl_4$, 97%, Sigma-Aldrich), palladium acetate ($Pd(OAc)_2$, 99%, Sigma-Aldrich) and sodium sulfide (Na_2S, Merck, 99%) were used as received.

2. Synthesis of TiO_2 and TiON

For synthesizing the TiON, $TiCl_4$ (7.43 mL, 48.6 mmol) was added dropwise to Na_2S solution (140 mL, 51.2 mmol). The pH of solution was adjusted to approximately 8 by dropwise addition of NH_3. The precipitate was continuously stirred for 5 h, then filtered and washed several times with distilled water to remove the chloride and sulfide ions [24]. The final product was calcined at 400 °C for 4 h in air condition. TiO_2 was also synthesized by this procedure but the Na_2S was not used [24].

3. Synthesis of a Binary Pd/TiON Nanocomposite

First, 0.02 mg of $Pd(OAc)_2$ was added into 50 mL of distilled water, then placed in an ultrasonic bath for 30 min. Afterwards, TiON powder (500 mg) was added to this solution and stirred at 80 °C. Under this condition, aqueous $NaBH_4$ solution (50 mL, 1.0 g) was added dropwise to the suspension. After ageing for 10 h, the solid product was collected by centrifuging and then washed with distilled water. Finally, this powder was dried overnight in a vacuum oven at 60 °C.

4. Synthesis of a Ternary Pd-GO/TiON Nanocomposite

GO nanosheets were synthesized according to the Hummers method [25,26]. Pd/GO was also synthesized according to previously reported protocol [27]. Pd-GO/TiON nanocomposite was synthesized in one step using TiON, Pd-GO and deionized water. An aqueous dispersion of Pd-GO was prepared by mixing of 10 mg Pd-GO in 100 mL of distilled water. Then, 10 mg of TiON was dispersed in 20 mL of distilled water and sonicated in an ultrasonic bath for 30 min. Afterwards, TiON dispersion was added to Pd-GO dispersion and stirred for 14 h at room temperature to obtain a homogeneous solution. The precipitate was filtrated and dried in vacuum oven at 50 °C for 4 h [28].

5. Preparation of Photocatalytic Nanocomposite Membranes (PhNMs)

The different quantities of each component for preparation of the PhNMs are given in Table 1. First, PVDF was added to DMF solvent and stirred for 5 h at 60 °C. After the relative dissolution of PVDF, photocatalytic agent was added to the polymeric solution and allowed to be stirred for 24 h. After removing the bubbles of polymeric solution by a vacuum pump, this polymeric solution was cast on a glass plate using Dr. Blade (200 μm) and then, immediately immersed in a deionized water bath and kept in distilled water at room temperature.

6. Photocatalytic Suzuki Reaction in Heterogeneous System

The desired amount of water (10 mL), aryl halide (1 mmol), aryl boronic acid (1.2 mmol), K_2CO_3 (2.5 mmol), SDS (1.0 mmol) and catalyst (Pd-TiON (5 mg) or Pd-GO/TiON (3 mg) or Pd (2 mg)) was mixed in a 25 mL round bottom flask. The photocatalytic reaction under visible light irradiation was conducted with an LED light bar in the wavelength range 400-700 nm (10 W, 30 pcs) in water bath at 25 °C. The distance between the LED light bar and flask was 25 cm. The yield of reaction was determined by gas chromatography.

Table 1. Composition of the prepared photocatalytic nanocomposite membranes

Samples	PVDF(g)	Pd-GO/TiON (g)	Pd-TiON (g)	DMF (g)
A	0.6	---	---	4
AI(1%)	0.6	0.006	---	4
AII(2%)	0.6	0.012	---	4
AIII(3%)	0.6	0.018	---	4
AIV(4%)	0.6	0.024	---	4
BI(1%)	0.6	---	0.006	4
BII(2%)	0.6	---	0.012	4
BIII(3%)	0.6	---	0.018	4
BIV(4%)	0.6	---	0.022	4



(a) (b)

Fig. 1. The filtration cell in (a) turn-off and (b) turn-on LED state.

7. Photocatalytic Suzuki Reaction using the Prepared Photocatalytic Nanocomposite Membranes

The performance of the prepared photocatalytic nanocomposite membranes for the Suzuki reaction was investigated using a dead-end filtration system. The membrane reactor cell is shown in Fig. 1. An LED strip in the wavelength range 400-700 nm as a visible light source was wrapped around the filtration cell. To activate the photocatalyst, the related nanocomposite membrane was exposed to visible light for 15 min before performing the Suzuki reaction. Afterwards, the desired amount of aryl halide (1 mmol), aryl boronic acid (1.2 mmol), K_2CO_3 (2.5 mmol) and SDS (1.0 mmol) was mixed with 10 mL of water and sonicated for 20 min. Then, this solution was poured into the filtration cell and exposed to visible light for 20 min. By applying a pressure of 4 bar, this solution passed through the membrane bulk and was exposed to the photocatalyst nanoparticles within the membrane. For yield of Suzuki reaction, concentration of products in permeate was analyzed by gas chromatography.

8. Flux Determination

Pure water flux (PWF) of all membranes was also measured by aforementioned dead-end filtration cell. Before measurement of PWF, all membranes were kept in deionized water for 24 h and then pre-pressurized at 0.4 MPa for 15 min in a dead-end cell to stabilize the membrane state. All permeation tests and photocatalytic reaction were performed at room temperature and at a pressure of 0.4 MPa. Pure water flux (J) ($Lm^{-2}h^{-1}$) was calculated by the following equation:

$$J=V/At \quad (1)$$

where V is the volume of the permeate (L), A is the touchable surface area (4.91×10^{-4} m^2) and t is the permeation time (h).

9. Characterization

A PL thermogravimetric analyzer (TGA 1000, UK) was employed to determine thermal stability of all samples in the range of 25-800 °C at the heating rate of 10 °C min^{-1}. The morphology of all samples was monitored by field emission scanning electron microscopy (FESEM) (Zeiss SUPRA 35VP). The modification of TiO_2 was characterized by (Gammadata-scienta ESCA 200) X-ray photoelectron spectroscopy (XPS). XPS was done in an ESCA/AES system equipped with a concentric hemispherical analyzer (CHA, Specs model EA10 plus). The data acquisition was at a nominal resolution of 0.1 eV. For exciting the X-ray photoelectrons, we used Al Kα line at 1,486.6 eV. The energy scale was calibrated against the carbon binding energy (284.6 eV). Before data acquisition, the samples were degassed for 3 h at 298 K under a pressure of 1.0×10^{-9} Torr to minimize surface contamination. X-ray diffraction (XRD) spectra (X-ray diffraction instrument (Siemens D5000) with a Cu target (λ=0.1540 nm) at room temperature) was used to study the crystalline structure of TiO_2-based photocatalyst samples. This instrument included a rotating anode generator which operated at 35 kV and 20 mA. The samples were scanned from 2θ=10 to 80° at the step scan mode; the diffraction pattern was recorded using a scintillation counter detector. The ultraviolet (UV)-visible diffuse reflectance spectroscopy (DRS) spectra were recorded with a Shimadzu MPC-2200 spectrophotometer.

RESULTS AND DISCUSSION

Due to poor photocatalytic activity of TiO_2 nanoparticles in the visible wavelength, N-doping of TiO_2 nanoparticles and use of GO nanosheets are considered to attain high performance photocatalyst in the visible region. Referring to the literature [28], GO nanosheets can act as suitable species to accept and transport the electrons from TiON photocatalyst under light irradiation. In addition, it has been reported that Pd nanoparticles as an effective catalyst for Suzuki reaction and GO as an electron reservoir reinforce the interfacial contact between Pd nanoparticles and photocatalyst, thereby providing a desirable transfer pathway of electrons between the interface of Pd nanoparticles and photocatalyst [19]. Therefore, in this work, a multifunctional efficient photocatalyst consisting of the TiO_2 photocatalyst, GO nanosheets and the catalytically active Pd-noble metal nanoparticles was synthesized to prepare effective PhNMs as suitable supports containing photocat-

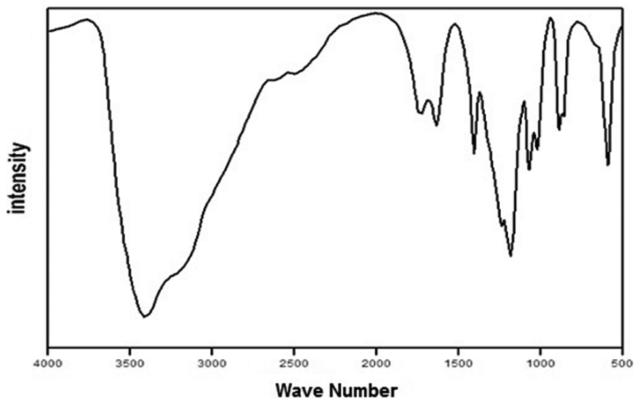


Fig. 2. FTIR spectrum of GO nanosheets.

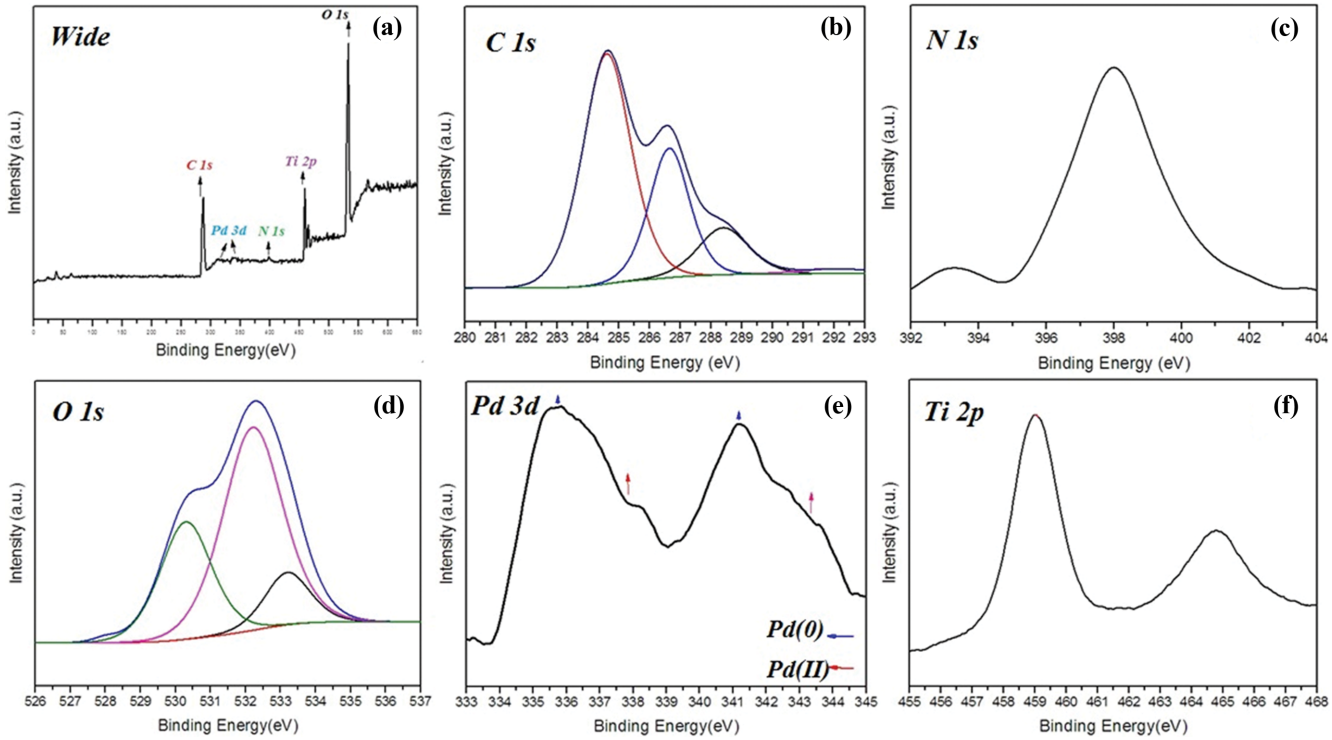


Fig. 3. (a) Wide scan XPS spectra of Pd-GO/TiON nanocomposite, (b) high-resolution XPS spectra of C1s peak, (c) N 1s peak, (d) O 1s peak, (e) Pd 3d peak and (f) Ti 2p peak in Pd-GO/TiON nanocomposite.

alyst for Suzuki coupling reactions under visible light irradiation. The synthesis of GO nanosheets was investigated by FTIR analysis. FTIR spectrum of GO is shown in Fig. 2. The characteristic peaks related to the hydroxyl and carbonyl groups appeared at around 3,400-3,500 and 1,727 cm^{-1}, respectively [26,23]. Moreover, several peaks observed at 1,066 and 1,400 cm^{-1} are attributed to C-O absorption band and C=O symmetric stretching vibration, respectively [23,26].

A careful analysis of the Pd-GO/TiON nanocomposite by XPS, EDX and EDX mapping provided evidence that synthesis of this photocatalyst was successful. To characterize the chemical composition of the synthesized photocatalyst, XPS analysis is considered as a powerful technique. Fig. 3(a) is the wide scan XPS spectra of Pd-GO/TiON nanocomposite, which illustrates the characteristic signal of C, O, Ti, N, and Pd elements. Fig. 3(b) shows the bonding energy of C 1s of GO; this peak can be deconvoluted in three particular peaks at 284.6 eV for C-C/C=C, 286.5 eV for C-OH, and 287.9 eV for O=C-OH, respectively [29]. This observation more confirms the synthesis of GO nanosheets. As can be seen in Fig. 3(c), unlike general XPS, peak for N 1s appeared at 400 eV; this peak was observed at 398.2 eV for N-doped TiO_2 which confirms the consolidation of the N-anion in TiO_2 [24]. Likewise, the characteristic peaks observed at 532.0 eV and 533.5 eV are assigned to O 1s (Fig. 3(d)), which can belong to functional groups containing oxygen atom bonded with C atoms of GO such as -OH and -COOH [29]. Moreover, the peak at 530 eV is related to O 1s of titanium-bound oxygen in TiON [24]. The binding energies observed with a spin-orbit gap of 5.3 eV at 335.4 eV and 340.7 eV (Fig. 3(e)) belong to Pd 3d3/2 and Pd 3d5/2, respectively, which reveals the existence of metallic Pd(0) [19]. As shown in (Fig. 3(e)), there are two shoulders in 338.5 eV and 343.5 eV which belong to Pd^{2+}. However, the high intensity peak of Pd(0) in comparison with Pd^{2+} manifests that high amount of Pd^{2+} was reduced to Pd(0). Ti 2p3/2 core level peaks of TiON sample appear at 458.5 eV (Fig. 3(f)). A low binding energy of Ti 2p in TiON sample compared with TiO_2 reveals the successful synthesis of TiON. XPS analysis obviously corroborated that the electronic interaction of Ti with anions is distinctly different from TiO_2 [24].

XRD analysis was performed to imply synthesis of GO nanosheets and immobilization of TiON/Pd onto Go nanosheets. As

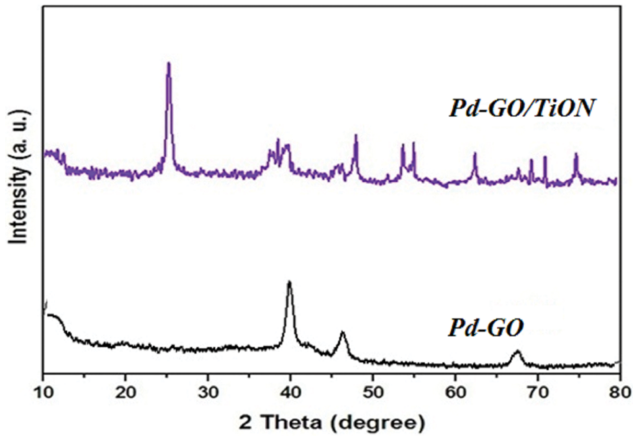


Fig. 4. XRD pattern of the Pd-GO (black graph) and the Pd-GO/TiON nanocomposites (purple graph).

shown in Fig. 4 (black and purple graph), a main peak at 11° is shown for GO nanosheets which confirms the synthesis of GO nanosheets [23]. This peak was also observed in other samples with lower intensity. The decline in intensity of GO peak and appearance of several new peaks in XRD patterns of modified GO nanosheets corroborates the attachment of TiON and Pd nanoparticles onto GO nanosheets. The XRD patterns of Pd-GO nanocomposite show several peaks at 40.10°, 46.60° and 60.20° which belong to the (111), (200) and (220) diffractions of crystalline Pd, respectively [19]. This observation can represent the presence of the metallic Pd with the fcc structure, which is shown in the purple graph with less intensity. As implied by Fig. 4 (purple graph), the XRD pattern of Pd-GO/TiON represents the existence of the anatase phase (25°) in the TiON crystal structure [30]. In addition, by considering the index peak at 25° for Pd-GO/TiON and 40.10° for Pd-GO, the sizes of the palladium and TiON nanoparticles was calculated by Debye Scherrer equation around 30 and 35 nm, respectively.

In addition, the elemental mapping by EDX was used to detect surface covering of GO nanosheets with Pd and TiON and their distribution on GO nanosheets. As can be seen in Fig. 5(a), (b) and (c), the EDX mapping shows a uniform distribution of Pd elements for Pd-GO and N, Pd and Ti elements for Pd-TiON and Pd-GO/TiON nanocomposites, respectively. The presence of C and O belongs to GO nanosheets as also manifested by this analysis. The presence of Ti and Pd can be clearly observed and confirmed by EDX patterns of Pd-GO and Pd-GO/TiON nanocomposites. However, the presence of N element is not clearly observed in EDX pattern of TiON nanocomposite, which can be attributed to less sensitivity of this analysis to detecting low content of elements. Thus XPS analysis was applied to more study of Pd-GO and Pd-GO/TiON nanocomposites. Complete explanations of XPS analysis are provided in the above section.

Absorption ability of N-doped TiO_2 in the visible light region and its absorption shift compared with TiO_2 were studied by DRS. DRS of TiON and TiO_2 are shown in Fig. 6. Blue and black lines show TiO_2 and TiON absorbance properties, respectively. As shown in Fig. 6, the absorption region for TiON is significantly higher than the TiO_2 in the visible region. It is clearly observed that the visible light absorption tails up to 800 nm in TiON. The inset curves distinctly show a different band gap energy for TiON compared with TiO_2. For TiON in comparison with TiO_2, an obvious decrease in the band gap of the valence band on TiON is illustrated. Also, a specific shift from ultraviolet area to the visible area is observed about 0.19 eV in the optical absorption range of TiON in compari-

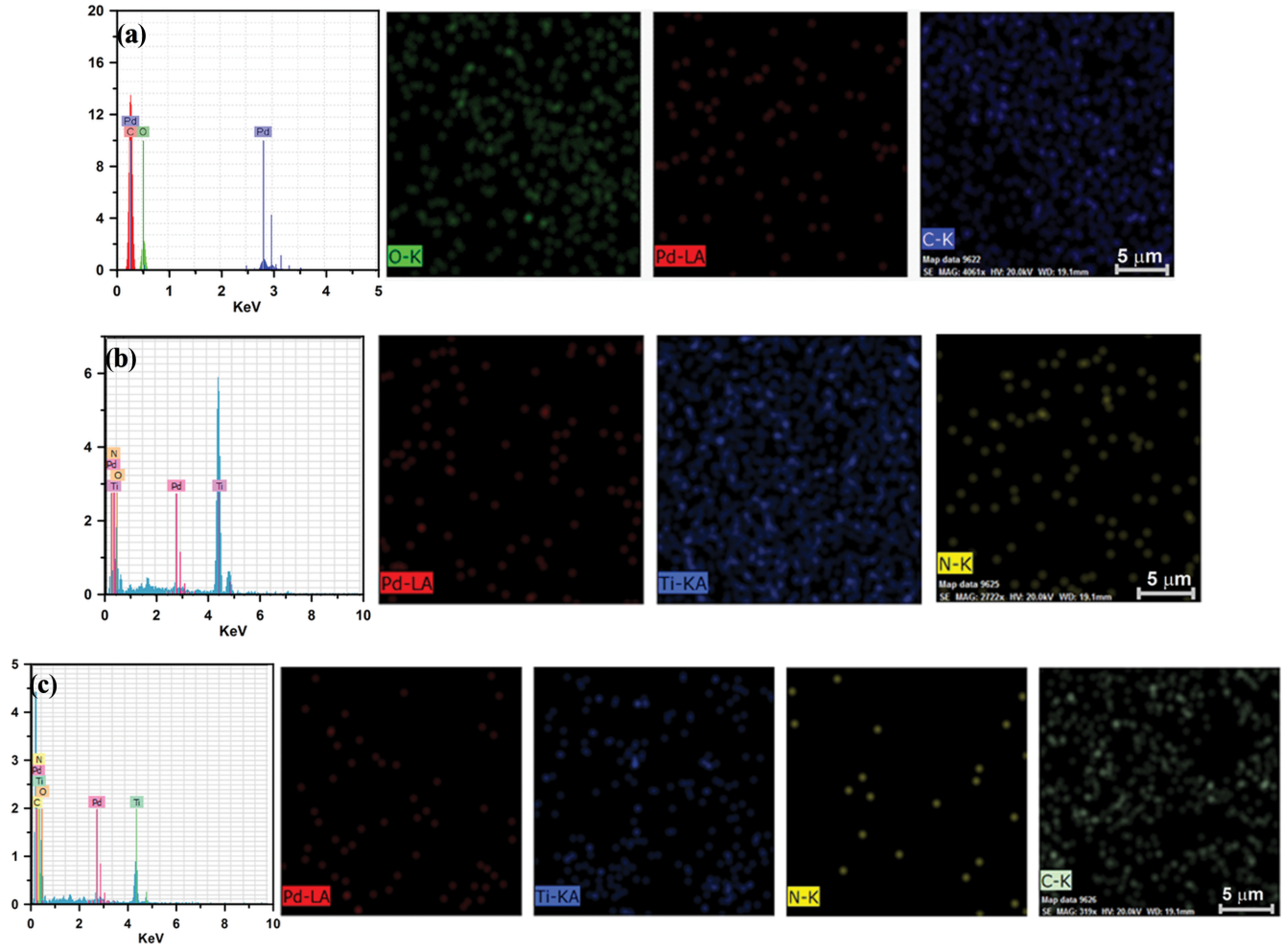


Fig. 5. EDX spectrum and EDX mapping of (a) the Pd-GO, (b) the Pd-TiON and (c) the Pd-GO/TiON nanocomposites.

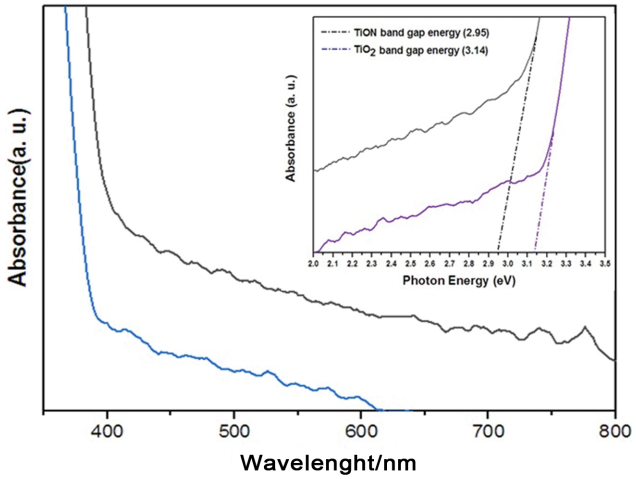


Fig. 6. DRS and transformed diffuse reflectance spectra (inset curve in Fig. 6).

son with TiO_2. This phenomenon can be attributed to the presence of nitrogen in the TiO_2 structure [24,31].

The results from previous analysis were corroborated by SEM analysis. The morphologies of the synthesized materials were characterized by SEM. The SEM images of Pd-GO and TiON nanocomposites are illustrated in Fig. 7(b) and 7(c). Comparing SEM images of GO and modified GO obviously reveals the changes of GO nanosheets surface in Fig. 7(a) and 7(b). Observation of a smooth surface for GO nanosheets in comparison with Pd immobilized GO nanosheets is well reflected in Fig. 7(a)-(b). Moreover, as can be seen in Fig. 7(b) and 7(c), spherical nanoparticles on the surface of GO nanosheets belonging to Pd nanoparticles are clearly manifesting the immobilization of Pd on the surface of GO nanosheets. From Fig. 7(b) and 7(c), the size of the Pd and TiON nanoparticles is in the range of about 30-40 nm and 45 nm, respectively. SEM images of Pd/GO nanocomposite are in good agreement with XPS results. These results confirm that Pd nanoparticles have

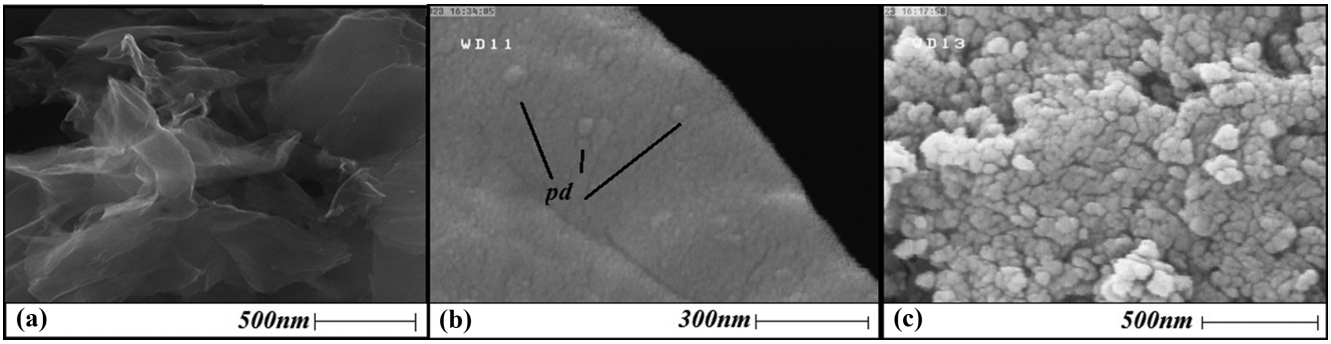


Fig. 7. SEM images of the (a) GO, (b) Pd-GO and (c) TiON nanoparticles.

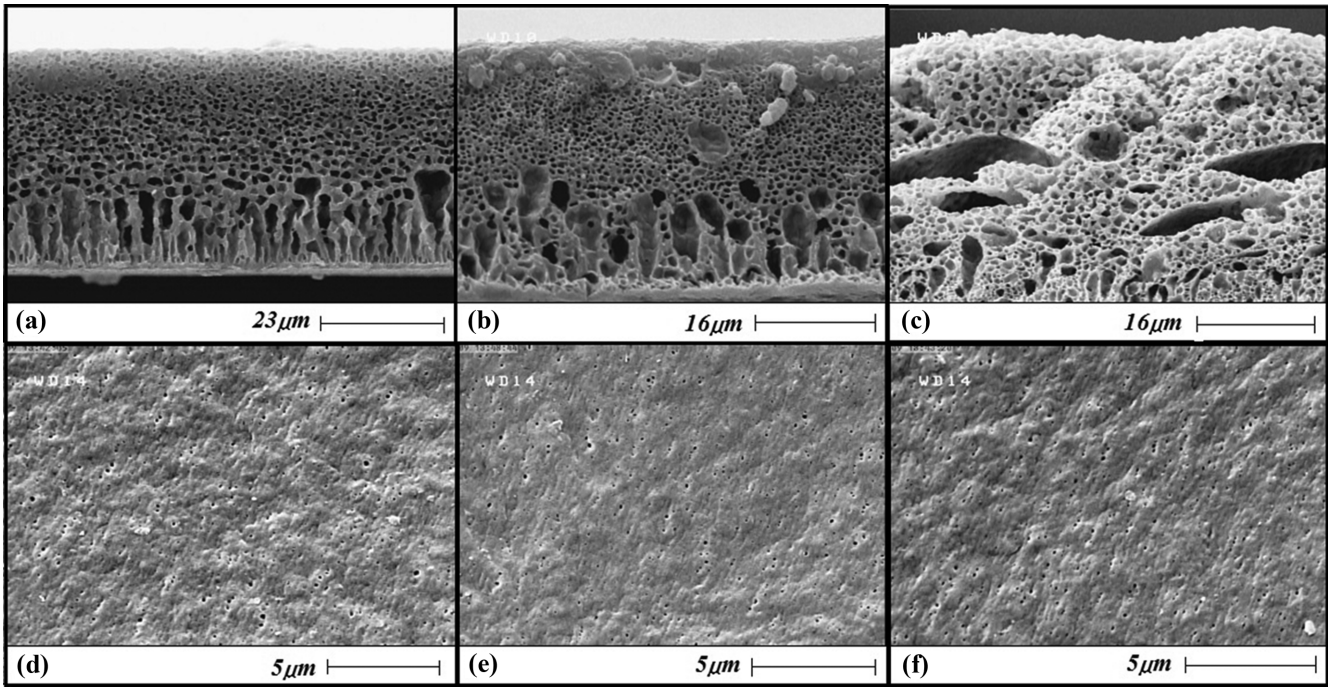


Fig. 8. SEM images of the cross section of (a) A, (b) AIV, (c) BIII, and top-layer surface of (d) A, (e) AIV and (f) BIII samples.

been successfully immobilized on the GO surface. The well distributed Pd nanoparticles with spherical shape onto the surface of GO nanosheets are also observed by SEM images and imply the EDX mapping results.

Fig. 8 shows the morphology of PVDF and PVDF nanocomposite membranes. For PVDF containing 4% Pd-GO/TiON (AIV) (Fig. 8(b)), an obvious increase in the number of the finger-like structures and also a size enlargement of the cavities compared to PVDF membrane (Fig. 8(a)) is illustrated. Morphology changes can be attributed to the addition of Pd-GO/TiON and its hydrophilic nature [32]. As can be seen in Fig. 8(c), SEM images demonstrate more and larger cavities for PVDF filled with 3% Pd-TiON (BIII) in comparison with other samples. Adding of TiON nanoparticles in the membrane resulted in the formation of this cavity due to the hydrophilic property of the TiON nanoparticles. In fact, the exchange rate of the solvent and non-solvent (distilled water) during the phase inversion process can be affected by addition of TiON nanoparticles [33]. Thus, adding of the hydrophilic TiON nanoparticles increases the exchange rate of the solvent and non-solvent, thereby forming larger cavities. Top-layer surface of the prepared nanocomposite membranes was also monitored by SEM images to detect the effect of the addition of TiO_2-based photocatalyst nanoparticles. The appearance of more pores on the top surface of the nanocomposite membranes also confirms the morphology changes due to the addition of nanoparticles [13]. Furthermore, as shown in Fig. 8(e), the presence of GO nanosheets contributes to the collapse of the symmetry in the porous structure and reduces the number of pores but increases the flux (Fig. 9) due to an increase in the average pore size [13].

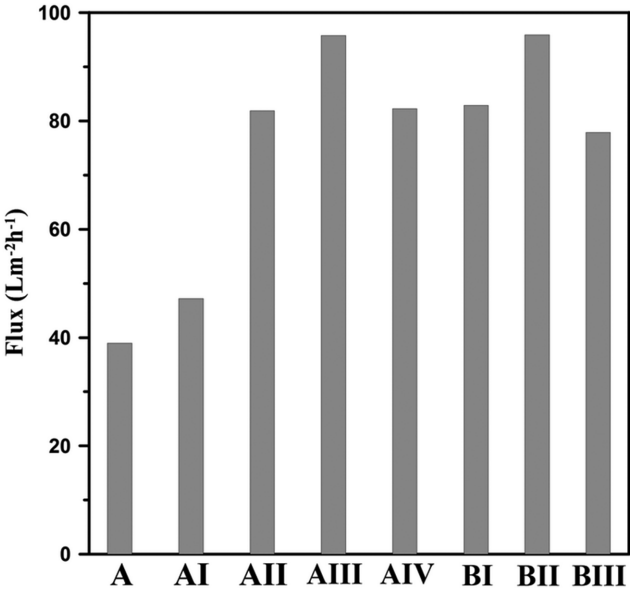
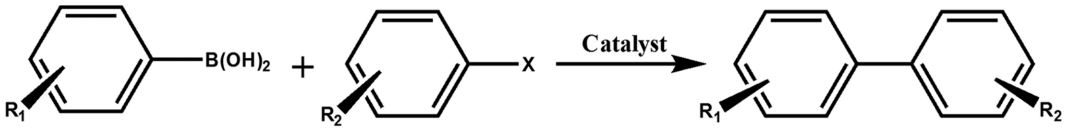


Fig. 9. PWF data of PVDF membrane and its nanocomposite membranes.

Changes in the morphology of PVDF-based nanocomposite membranes are more confirmed by PWF (Pure Water Flux) data. As shown in Fig. 9, by adding TiO_2-based photocatalytic nanoparticles, PWF of nanocomposite membranes dramatically increases by increasing nanoparticles loading within PVDF matrix. In correlation with the SEM images, PWF data reveals the significant increase in porosity and cavity size of nanocomposite membranes compared with PVDF (see SEM images). As can be seen in Fig. 9, a significant increase in PWF is observed when the fraction of Pd-TiON and Pd-GO/TiON nanoparticles is increased up to 2 and 3 wt% in the PVDF-based nanocomposite membranes; however, the nanocomposite membranes containing higher nanoparticles loading demonstrated a reduction in PWF. As described above, the PWF enhancement can be attributed to hydrophilic nature of nanoparticles [13,34]. But, decreasing of PWF in higher nanoparticles content resulted from the accumulation of nanoparticles and blockage of membrane pores with nanoparticles [13,32]. In addition, as can be seen in Fig. 9, pore-filling of nanocomposite membrane containing Pd-TiON occurred in low nanoparticle content in comparison with nanocomposite membranes filled with Pd-GO/TiON, which is due to the smaller size of Pd-TiON nanoparticles compared with Pd-GO/TiON. The large size of Pd-GO/TiON nanoparticles is related to the large dimensions of GO nanosheets used as support for Pd and TiON nanoparticles. Therefore, high content of Pd-TiON (4 wt%) was not more investigated due to undesirable effects of Pd-TiON nanoparticles on PWF of the related nanocomposite membranes.

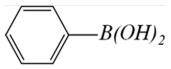
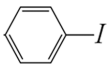
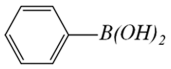
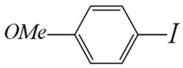
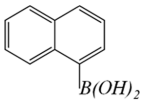
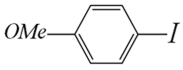
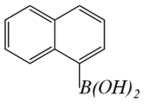
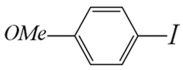
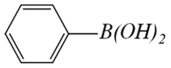
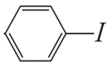
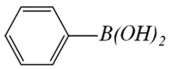
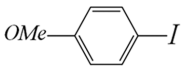
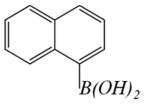
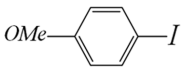
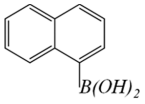
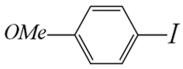
Nanocomposite membranes containing 3% Pd-GO/TiON (AIII) and 3% Pd-TiON (BIII) were selected to evaluate the photocatalytic performance. Photocatalytic performance of the prepared nanocomposite membranes was evaluated for Suzuki coupling reaction (Scheme 1).

The efficiency and rate of this reaction depends on the type of halogen substituent of aryl halide compounds (I, Br, Cl) and the position and type of the substituent groups (electron-withdrawing or donating-electron groups) used for that [35]. Therefore, different types of aryl bronic acid and aryl halide compounds were utilized to assess photocatalytic performance of the prepared nanocomposite membranes. It is known that the effect of the halogen substituent in Suzuki coupling reaction rate is as follows I>Br>Cl. Therefore, in this work, aryl iodide was only used for photocatalytic assay of the prepared nanocomposite membranes. Yield of Suzuki coupling reaction for different components is presented in Table 2. High efficiency and high reaction rate for Suzuki coupling reaction are achieved when aryl halide compounds have electron-withdrawing groups [19]. From Table 2, it is observed that PVDF@Pd-GO/TiON was a more efficient photocatalytic mem-



Scheme 1. Suzuki coupling reaction.

Table 2. Photocatalytic performance results of the prepared nanocomposite membranes in Suzuki-Miyaura coupling reactions

Samples	Aryl halides	Arylboronicacids	Yield (%)
AIII			70
AIII			66
AIII			67
AIII			65
BIII			65
BIII			60
BIII			49
BIII			55

brane for Suzuki coupling reaction, especially when naphthalene-1-boronic acid was used. This result clearly reveals the synergy effect of GO on Pd-TiON. Hence, the higher yield of this nanocomposite membrane in respect to the other nanocomposite membranes can be attributed to the synergy effect of GO on Pd-TiON. In addition, this can result from the π-π interaction between GO nanosheets and naphthalene-1-boronic acid [36].

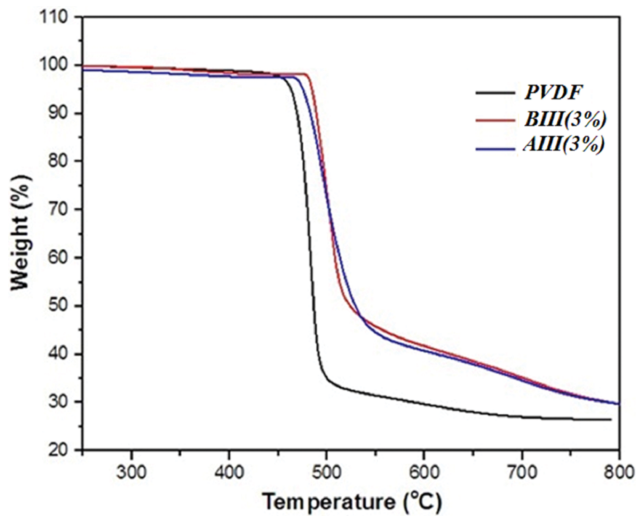


Fig. 10. TGA curves of PVDF and its nanocomposites.

The thermal stability of AIII and BIII nanocomposite membranes was studied by TGA analysis (Fig. 10). From TGA results, a significant improvement in the temperature degradation and ash content of PVDF-based nanocomposite membrane was detected. Enhancement of thermal stability of the nanocomposite membrane in comparison with neat PVDF is mainly attributed to the hydrogen-bonding interaction between the PVDF chains and the polar group of Pd-TiON and Pd-GO/TiON [13,37]. Additionally, for nanocomposite membrane containing Pd-GO/TiON nanoparticles, the barrier effect of GO nanosheets can delay thermal transport in PVDF matrix, thereby improving thermal stability of nanocomposite membranes.

CONCLUSIONS

Recovery and reutilization of catalyst are important factors and fundamental issues in synthetic chemistry and green chemistry approach. Therefore, in this work, designing of PVDF@Pd-GO/TiON as a photocatalytic nanocomposite membrane was considered to overcome these aspects. Use of membrane process can be promising in the chemical industry due to reduced costs of the separation process, reduction of production stages and decrease of environmental damage. Nitrogen doping of TiO_2 in combination with use of GO nanosheets and Pd element was employed to prepare the visible-light sensitive TiO_2-based photocatalysts in which is used the fabrication of photocatalytic nanocomposite membranes. The reduction of band gap of the TiON compared with TiO_2 is manifested by DRS analysis. In addition, the anion doping of TiO_2 with nitrogen element and the presence of Pd(0) in the synthesized nanocomposite photocatalyst were confirmed by XPS analysis. An efficiency of more than 70% and 99% was obtained in evaluation of Pd-GO/TiON as photocatalyst for Suzuki reaction in heterogeneous system and the prepared photocatalytic nanocomposite membranes containing 3% Pd-GO/TiON, respectively.

REFERENCES

1. J. Kim and B. van der Bruggen, *Environ. Pollut.*, **158**, 2335 (2010).
2. L. Qiu, X. Zhang, W. Yang, Y. Wang, G. P. Simon and D. Li, *Chem. Commun.*, **47**, 5810 (2011).
3. P. Aerts, S. Kuypers, I. Genne, R. Leysen, J. Mewis, I. Vankelecom and P. Jacobs, *J. Phys. Chem. B*, **110**, 7425 (2006).
4. H. Strathmann, *AIChE J.*, **47**, 1077 (2001).
5. A. Tiraferri, C. D. Vecitis and M. Elimelech, *ACS Appl. Mater. Interfaces*, **3**, 2869 (2011).
6. B. J. Hinds, N. Chopra, T. Rantell, R. Andrews, V. Gavalas and L. G. Bachas, *Science*, **303**, 62 (2004).
7. M. Brettreich, S. Burghardt, C. Böttcher, T. Bayerl, S. Bayerl and A. Hirsch, *Angew. Chem. Int. Ed.*, **39**, 1845 (2000)
8. X. Zhao, L. Lv, B. Pan, W. Zhang, S. Zhang and Q. Zhang, *Chem. Eng. J.*, **170**, 381 (2011).
9. L. Y. Ng, A. W. Mohammad, C. P. Leo and N. Hilal, *Desalination*, **308**, 15 (2013).
10. S. Prakash, C. Charan, A. K. Singh and V. K. Shahi, *Appl. Catal. B. Environ.*, **132**, 62 (2013).
11. M. Buonomenna, S. Choi and E. Drioli, *Asia-Pac. J. Chem. Eng.*, **5**,

26 (2010).
12. J. Shu, B. Grandjean, A. V. Neste and S. Kaliaguine, *Can. J. Chem. Eng.*, **69**, 1036 (1991).
13. H. Mahdavi, A. Rahimi and L. Ahmadian Alam, *Polym. Bull.*, **74**, 3557 (2017).
14. R. Molinari, L. Palmisano, E. Drioli and M. Schiavello, *J. Membr. Sci.*, **206**, 399 (2002).
15. U. Diebold, *Appl. Phys. A*, **76**, 681 (2003).
16. K. Hashimoto, H. Irie and A. Fujishima, *Jpn. J. Appl. Phys.*, **44**, 8269 (2005).
17. R. Daghrir, P. Drogui and D. Robert, *Ind. Eng. Chem. Res.*, **52**, 3581 (2013).
18. J. Park, J.-Y. Lee and J.-H. Cho, *J. Appl. Phys.*, **100**, 113534 (2006).
19. Y. Li, Z. Zhang, L. Pei, X. Li, T. Fan, J. Ji, J. Shen and M. Ye, *Appl. Catal. B Environ.*, **190**, 1 (2016).
20. Q. Li, Y. W. Li, P. Wu, R. Xie and J. K. Shang, *Adv. Mater.*, **20**, 3717 (2008).
21. Q. Li, R. Xie, E. A. Mintz and J. K. Shang, *J. Am. Ceram. Soc.*, **90**, 3863 (2007).
22. G.-d. Kang and Y.-m. Cao, *J. Membr. Sci.*, **463**, 145 (2014).
23. Y. Zhu, S. Murali, W. Cai, X. Li, J. W. Suk, J. R. Potts and R. S. Ruoff, *Adv. Mater.*, **22**, 3906 (2010).
24. M. Sathish, B. Viswanathan, R. Viswanath and C. S. Gopinath, *Chem. Mater.*, **17**, 6349 (2005).
25. W. S. Hummers Jr. and R. E. Offeman, *J. Am. Chem. Soc.*, **80**, 1339 (1958).
26. L. Ahmadian-Alam, M. Teymoori and H. Mahdavi, *J. Polym. Res.*, **25**, 13 (2018).
27. G. M. Scheuermann, L. Rumi, P. Steurer, W. Bannwarth and R. Mülhaupt, *J. Am. Chem. Soc.*, **131**, 8262 (2009).
28. T.-D. Nguyen-Phan, V. H. Pham, E. W. Shin, H.-D. Pham, S. Kim, J. S. Chung, E. J. Kim and S. H. Hur, *Chem. Eng. J.*, **170**, 226 (2011).
29. S. Stankovich, D. A. Dikin, R. D. Piner, K. A. Kohlhaas, A. Kleinhammes, Y. Jia, Y. Wu, S. T. Nguyen and R. S. Ruoff, *Carbon*, **45**, 1558 (2007).
30. K. Thamaphat, P. Limsuwan and B. Ngotawornchai, *Kasetsart J., (Nat. Sci.)*, **42**, 357 (2008).
31. M. Mollavali, C. Falamaki and S. Rohani, *Int. J. Hydrogen Energy*, **40**, 12239 (2015).
32. C. Zhao, X. Xu, J. Chen and F. Yang, *J. Environ. Chem. Eng.*, **1**, 349 (2013).
33. S. J. Oh, N. Kim and Y. T. Lee, *J. Membr. Sci.*, **345**, 13 (2009).
34. X. Cao, J. Ma, X. Shi and Z. Ren, *Appl. Surf. Sci.*, **253**, 2003 (2006).
35. G. M. Scheuermann, L. Rumi, P. Steurer, W. Bannwarth and R. Mülhaupt, *J. Am. Chem. Soc.*, **131**, 8262 (2009).
36. D. Pacilé, J. Meyer, A. F. Rodríguez, M. Papagno, C. Gomez-Navarro, R. Sundaram, M. Burghard, K. Kern, C. Carbone and U. Kaiser, *Carbon*, **49**, 966 (2011).
37. L. Y. Yu, H. M. Shen and Z. L. Xu, *J. Appl. Polym. Sci.*, **113**, 1763 (2009).